Impacts of biomass burning and photochemical processing on the light absorption of brown carbon in the southeastern Tibetan Plateau

Jie Tian[1,2], Qiyuan Wang[1,2], Yongyong Ma[3], Jin Wang[1], Yongming Han[1,2], and Junji Cao[1,4]

[1]Key Laboratory of Aerosol Chemistry and Physics, State Key Laboratory of Loess and Quaternary Geology, Institute of Earth Environment, Chinese Academy of Sciences, Xi'an 710061, China
[2]CAS Center for Excellence in Quaternary Science and Global Change, Xi'an 710061, China
[3]Meteorological Institute of Shaanxi Province, Xi'an 710015, China
[4]Institute of Atmospheric Physics, Chinese Academy of Sciences, Beijing 100029, China

Correspondence: Qiyuan Wang (wangqy@ieecas.cn) and Junji Cao (jjcao@mail.iap.ac.cn)

Abstract. Brown carbon (BrC) in the atmosphere can greatly influence aerosol's radiative forcing over the Tibetan Plateau (TP), because it has the non-negligible capacity of light absorption compared to black carbon (BC); however, our understanding of optical properties, sources, atmospheric processes of BrC in this region remains limited. In this study, a multiple-wavelength Aethalometer coupled with a quadrupole aerosol chemical speciation monitor were deployed to investigate the highly time resolved BrC in the submicron aerosol in the southeastern edge of the TP during the pre-monsoon season. The result showed that BrC had the substantial contributions (20.0–40.2 %) to the light absorption of submicron aerosol from 370 to 660 nm. Organic aerosol (OA), an alternative to BrC, was split into a biomass burning OA (BBOA) with aging process and a photochemical-oxidation processed oxygenated OA (po-OOA) by a hybrid environmental receptor model analysis. Combined with light absorption coefficient of BrC ($b_{abs\text{-}BrC}$), the source-specific mass absorption cross section of BBOA (0.61−2.78 $m^2\ g^{-1}$) and po-OOA (0.30−1.43 $m^2\ g^{-1}$) at 370−660 nm were retrieved. On average, $b_{abs\text{-}BrC}$ from po-OOA (1.3−6.0 Mm^{-1}) was comparable to that from BBOA (1.3−6.0 Mm^{-1}) at all wavelengths. The concentration weighted trajectory analysis showed that the most important potential source regions for $b_{abs\text{-}BrC}$ values from BBOA and po-OOA were located in the northern Myanmar and along the China-Myanmar border, indicating the cross-border transport of BrC from Southeast Asia. A "simple forcing efficiency" evaluation further illustrated the importance of BrC radiative effect with the high fractional radiative forcing by two OAs relative to BC (48.8 ± 15.5 %). This study highlighted a significant influence of BrC of biomass burning origin and secondary formation on climate change over the TP region during the pre-monsoon season.

1 Introduction

Carbonaceous aerosols, a major component of atmospheric particles, play an important role in the global climate by directly absorbing and scattering solar and terrestrial radiation (Bellouin et al., 2013; IPCC, 2013; Yao et al., 2017). In the past, black carbon (BC) was often considered to be the only light-absorbing carbonaceous aerosol, and organic aerosol (OA) was thought to purely scatter light (Bond and Bergstrom, 2006; Koch et al., 2007). However, a fraction of OA has been found to absorb radiation efficiently in near-ultraviolet (UV) and visible spectral ranges with a strong wavelength dependence (Kirchstetter et al., 2004). This light-absorbing OA, collectively known as brown carbon (BrC) (Andreae and Gelencsér, 2006), is receiving increasing attention due to its non-negligible radiative effect. Feng et al. (2013) and Lin et al. (2014) have reported that the radiative forcing (RF) caused by BrC absorption on a global scale can be up to + 0.25 and + 0.57 W m^{-2}, respectively. Zhang et al. (2020a) estimated that globally BrC contributed more than 25% of BC RF, wherein the atmospheric heating of BrC is greater than that of BC in the tropical mid and upper troposphere. Zhang et al. (2017) also suggested that the clear-sky RFs of high- and low-altitude BrC were 0.35 ± 0.16 and 0.65 ± 0.34 W m^{-2}, corresponding to 34% and 24% of carbonaceous aerosol warming effect at the tropopause, respectively. The inclusion of BrC in climate models can reduce uncertainties in the global or regional RF assessment of aerosols. Therefore, a comprehensive understanding on light absorption properties of BrC is required.

In the atmosphere, primary BrC is mainly emitted from biomass burning and fossil fuel combustion (Olson et al., 2015; Washenfelder et al., 2015; Xie et al., 2017), and secondary BrC is commonly formed from photochemical-oxidation and aqueous reactions of biogenic or anthropogenic precursors (Hecobian et al., 2010; Nakayama et al., 2013). The complex sources and formation mechanisms of BrC lead to the spatial-temporal variations in its light absorption properties. Accurately quantifying the source-specific absorption capacity (i.e., mass absorption cross section (MAC)) of BrC is essential for modelling BrC climate effect. However, direct source apportionment of BrC is impossible with current analytical method, since BrC constituents responsible for light absorption remain relatively unknown (Laskin et al., 2015). Recent studies have usually used OA as an alternative to BrC for two major reasons: (1) the definition of OA contains all BrC constituents, and (2) OA from either online monitoring or filter extraction can be apportioned to a few major primary and secondary sources with the development of mass spectrometry. This allows for establishing the relationship between primary and secondary OA types and BrC absorption, which provides better quantification of the impact of BrC from different sources and formation mechanisms on regional and global climates (Kaskaoutis et al., 2021; Moschos et al., 2018; Qin et al., 2018; Wang et al., 2021).

The Tibetan Plateau (TP), often referred to as the “Third Pole”, is the largest and highest mountain region in the world and contains the most abundant ice outside of the polar regions (Yao et al., 2012). It has a huge impact on the large-scale atmospheric circulation and the hydrological cycle, which is the most sensitive and visible indicator of climate change

in the entire Asian continent (Chen and Bordoni, 2014; Immerzeel et al., 2010). In the recent decades, there has been the growing evidence of increased surface temperature in the Himalayas and the TP regions, accompanied by the accelerated glacier melt and retreat (Kehrwald et al., 2008; Liu and Chen, 2000; Wang et al., 2008). This rapid warming was firstly attributed to greenhouse gas warming; however, light-absorbing aerosols were found to be another major warming agent (Lau et al., 2010; Ramanathan et al., 2007). Previous studies paid a large amount of attention on BC due to its vital climatic implication in the TP. The sources of BC varied significantly with the receptor location and the season (Kopacz et al., 2011; Tan et al., 2021; Zhang et al., 2015). For example, Zhang et al. (2015) reported that biomass burning from South Asia has the largest impact on BC in the central TP, while fossil fuel combustion contributed the most to BC burden in the northeast TP in all seasons and southeast TP in the summer. The direct RF of BC at the top of the atmosphere (+ 1.6−3.5 W m^{-2}) induced atmospheric heating rates of 0.13−0.35 K day^{-1} in the Himalayas and the TP regions (Liu et al., 2021; Panicker et al., 2020); meanwhile, BC deposited on the snow-covered areas can increase 1.0 ℃ of the surface temperature over the TP by reducing the snow albedo (Qian et al., 2011). It is clearly that there are primary OA emissions along with BC emitted from biomass burning and fossil fuel combustion, and secondary OA formation has been found in the TP (Xu et al., 2018; Zhang et al., 2019). However, the link between light absorption properties and sources of OA is less understood so far, which would lead to uncertainties in evaluating aerosol radiative effect of TP.

In this study, real-time measurements of both light absorption properties and chemical characteristics of submicron aerosol were conducted in the southeastern margin of the TP during the pre-monsoon season. The main objectives were to (1) characterize the light absorption properties of BrC, (2) quantify the source-specific MAC and absorption of BrC, and (3) evaluate the importance of BrC radiative effect from different sources. This study provides insights into light absorption properties of BrC, which is necessary for understanding the role of BrC in climate warming and revealing impacts of sources and atmospheric processes in the TP and surrounding areas.

2 Methodology

2.1 Sampling site and period

Submicron aerosol online measurements of optical and chemical properties were performed at the Lijiang Astronomical Station, Chinese Academy of Sciences, Gaomeigu County, Yunnan Province (26 °41' N, 100 °1' E; 3260 m a.s.l.) (Fig. 1). Continuous hourly O_3 and relative humidity (RH) were measured with the use of an ozone analyzer (EC9810, Ecotech Pty Ltd, Australia) and an automatic weather station (MAWS201, Vaisala, Helsinki, Finland). The monitoring station is situated in the southeastern edge of the TP, a natural channel for the transport of air pollutants from Southeast Asia to the TP (Tan et al., 2021). All instruments were placed on the rooftop of an office building (~10 m above the ground), without any strong anthropogenic emission sources nearby. More detailed description about the sampling site can be

found in Wang et al. (2019) and Liu et al. (2021). The sampling period lasted from 8:00 local stand time (LST, all time references that follow are given in LST) on 14 to 23:00 on 31 March, 2018, corresponding to the pre-monsoon season in the TP.

2.2 Submicron aerosol measurements

A newly developed Aethalometer (Model AE33, Magee Scientific, Berkeley, CA, USA) was used to measure aerosol light absorption coefficient (b_{abs}) at multiple wavelengths (i.e., 370, 470, 520, 590, 660, and 880 nm) with a 1 min time resolution. Briefly, the ambient air sampled at a flow rate of 5 L min^{-1} was firstly selected by a PM_1 (particulate matter with an aerodynamic diameter ≤ 1.0 μm) cyclone separator (BGI SCC 1.197, Mesa Labs, USA) to collect submicron aerosol on the filter. Light at different wavelengths emitted from diodes irradiated two parallel filter spots with deposition rates of 3.85 and 1.15 L min^{-1}, respectively. Thereafter, the two light attenuations measured by optical detectors was used to calculate b_{abs} through a real-time loading effect compensation algorithm. This "dual-spot" technique for the Model AE33 can eliminate the nonlinearity effect caused by increasing amount of aerosol deposit on the filter (Weingartner et al., 2003). Additionally, the Model AE33 automatically used a factor of 2.14 to compensate the scattering effect of quartz filter. Detailed operating principles of the Model AE33 can be found in Drinovec et al. (2015).

OA in the non-refractory PM_1 was measured using a quadrupole aerosol chemical speciation monitor (Q-ACSM, Aerodyne Research Inc., Billerica, Massachusetts, USA) with a 30 min time resolution. The aerodynamic lens coupled with a 100 μm diameter critical aperture in the Q-ACSM created a beam of focused submicron aerosols (40−1000 nm aerodynamic diameter), which was vaporized at ~600 ℃, ionized by a 70 eV electron impact, and subsequently characterized with a mass spectrometer. The details of the instrument have been described elsewhere (Ng et al., 2011b). The measured Q-ACSM data was processed by the ACSM local tool version 1.5.3.5 compiled with Igor Pro 6.37 (Wavemetrics, Inc., Lake Oswego, OR, USA) to determine the mass concentration and ion-speciated mass spectra of OA. Four our study, the default collection efficiency (0.45) and relative ionization efficiency (1.4) were used to obtain OA mass concentration (Middlebrook et al., 2012). The mass concentration and error matrices of organic fragments from mass-to-charge (*m/z*) 12 to 120 were initialized following the method of Allan et al. (2003).

2.3 Data analysis

2.3.1 Separation of BrC and BC absorption

The extrapolation method based on Absorption Ångström exponent (AAE) is widely used to project the absorption at the longer wavelength to the shorter wavelength of the spectrum (Olson et al., 2015; Pokhrel et al., 2017). With an assumption of b_{abs} at 880 nm (b_{abs} (880 nm)) solely from BC (Kirchstetter et al., 2004), the light absorption coefficient of BC ($b_{abs\text{-}BC}$) at wavelengths (λ) of 370, 470, 520, 590, and 660 nm can be obtained using the following formula:

$$b_{abs\text{-}BC}(\lambda) = b_{abs}(880\ nm) \times \left(\frac{880}{\lambda}\right)^{AAE_{BC}} \quad (1)$$

Here, b_{abs} and $b_{abs\text{-}BC}$ are given in inverse megameters (Mm^{-1}); AAE_{BC} is assumed to be 1.1 ± 0.3, which represents the likely range of AAE for BC externally and internally mixed with non-absorbing material (Lack and Langridge, 2013). Then, BrC absorption is derived by subtracting BC absorption from the total submicron aerosol absorption via:

$$b_{abs\text{-}BrC}(\lambda) = b_{abs}(\lambda) - b_{abs\text{-}BC}(\lambda) \quad (2)$$

Here, $b_{abs\text{-}BrC}$ is the light absorption coefficient of BrC (Mm^{-1}).

2.3.2 Hybrid environmental receptor model (HERM) analysis

HERM is an effective receptor model, which was performed to retrieve potential sources of OA in this study. The HERM algorithm groups the matrix X (measured mass spectra of organic fragments) into two nonnegative constant matrices G (source contribution) and F (mass spectra of specific sources), and the model residual matrix E, defined as:

$$X = G \times F + E \quad (3)$$

The model does not require prior mass spectra of sources, and the values of G and F can be obtained using an iterative conjugate gradient algorithm. The principle of HERM has been described in detail elsewhere (Chen and Cao, 2018).

Before HERM analysis, *m/z* from 12 to 120 with signal-to-noise between 0.2 and 2 and *m/z* 44 were down-weighted by increasing their errors by a factor of 2 (Ulbrich et al., 2009). HERM solutions from two to five factors with unconstrained mass spectrum were investigated to explore potential sources. The two-factor solution were chosen as the optimal solution, while greater number of factors (3−5) solutions existed many non-physical meaning factors dominated by individual *m/z* and do not further split new sources. Bootstrap (BS) method was adopted for two-factor solution (Brown et al., 2015). In 50 times BS, no mass spectrum was unmapped ($r < 0.6$) indicating the two-factor solution was robust. Therefore, a biomass burning OA (BBOA) and a photochemical-oxidation processed oxygenated OA (po-OOA) were finally identified. More detailed description of mass spectra, time series, and correlations with tracers of these two OA factors can be found in Sect. 3.2.

2.3.3 Calculation of optical parameters

The MAC of OA component in this study was resolved by the multiple linear regression (MLR) model combined with $b_{abs\text{-}BrC}$ and OA source apportionment results, which is defined as follows:

$$b_{abs\text{-}BrC}(\lambda) = a_1(\lambda) \times [BBOA] + a_2(\lambda) \times [po\text{-}OOA] \quad (4)$$

Here, a_1 and a_2 denote the MAC of BBOA (MAC_{BBOA}) and po-OOA ($MAC_{po\text{-}OOA}$), respectively, in square meters per gram ($m^2\ g^{-1}$); [BBOA] and [po-OOA] are the mass concentration of BBOA and po-OOA, respectively, in micrograms per cubic meter ($\mu g\ m^{-3}$). Tolerance (0.2) and variance inflation factor (4.7) for the ordinary least square fitting results

indicated that there was no serious multicollinearity between two independent variables, however, heteroscedasticity existed according to "White Test" ($p < 0.05$). Thus, the weighted least squares method was used for parameter estimation in MLR model. The MAC of BC (MAC_{BC}) was directly calculated with $b_{abs\text{-}BC}$ divided by the mass concentration of BC, which was obtained by dividing b_{abs} (880 nm) by the default MAC (880 nm) used in the Model AE33 (Drinovec et al., 2015).

AAE describes the spectral dependence of light absorption by aerosols, and it can be calculated using a power law function with b_{abs} and MAC, respectively:

$$b_{abs}(\lambda) = k_1 \times \lambda^{-AAE} \quad (5)$$

$$MAC(\lambda) = k_2 \times \lambda^{-AAE} \quad (6)$$

Here, k_1 and k_2 are constants independent of wavelength.

2.4 Trajectory-related analysis

A geographic information system based software TrajStat was utilized to investigate the influences of regional transport on BrC absorption at Gaomeigu from 14 to 31 March, 2018 (Wang et al., 2009). The trajectories were calculated with the Hybrid Single-Particle Lagrangian Integrated Trajectory (HYSPLT) model developed by the National Oceanic and Atmospheric Administration (Draxler and Hess, 1998). In this study, the model was set to run twenty-four times per day at starting times of 0:00−23:00 with 1 h step. 72-h backward trajectories at the height of 500 m above the ground level at Gaomeigu during the sampling period were produced based on the gridded meteorological data from Global Data Assimilation System (ftp://arlftp.arlhq.noaa.gov/pub/archives/gdas1, last access: 1 June, 2022).

The concentration weighted trajectory (CWT) method was further used to identify the potential source regions that likely affected the BrC absorption at Gaomeigu (Hsu et al., 2003). The geographic zone covered by the total number of backward trajectories (K) was divided into I × J grid cells with the resolution of 0.5 ° × 0.5 °. The CWT value of each grid can be defined as follows:

$$b_{abs\text{-}BrC\text{-}ij} = \frac{\sum_{k=1}^{K} b_{abs\text{-}BrC\text{-}k}\tau_{ijk}}{\sum_{k=1}^{K} \tau_{ijk}} W_{ij} \quad (7)$$

Here, $b_{abs\text{-}BrC\text{-}ij}$ is the average weighted light absorption coefficient of BrC in the *ij*th cell; $b_{abs\text{-}BrC\text{-}k}$ is the light absorption coefficient of BrC observed on the arrival of trajectory *k*; and τ_{ijk} is the time spent in the *ij*th cell by trajectory *k*. The weighting function of W_{ij} was applied to reduce the effect of the small number of back-trajectory segment endpoints that fall into the grid cell (Wang et al., 2006):

$$W_{ij} = \begin{cases} 1.00 & 135 < n_{ij} \\ 0.70 & 45 < n_{ij} \leq 135 \\ 0.42 & 15 < n_{ij} \leq 45 \\ 0.17 & n_{ij} \leq 15 \end{cases} \quad (8)$$

Here, n_{ij} is the total number of endpoints in the ijth cell. In this study, the total number of endpoints located in 72 cells of the geographic zone is 3268, so that the average number of endpoints in all cells is about 45.

2.5 Radiative effect calculation

The concept "simple forcing efficiency" (SFE) introduced by Bond and Bergstrom (2006) is a useful way to evaluate the radiative effect of atmospheric aerosols. Without consideration of aerosol scattering, a variant of wavelength-dependent SFE is given as follows:

$$SFE_i(\lambda) = \frac{S_0(\lambda)}{4} \times \tau_{atm}^2 \times (1 - F_c) \times [4a_s \times MAC_i(\lambda)] \quad (9)$$

Here, the subscript i represents BBOA, po-OOA, or BC; λ denotes the wavelength from 370 to 660 nm with 1 nm step; SFE is given in watts per gram (W g^{-1}), which represents the positive energy added to the Earth atmosphere system by a given mass of light-absorbing particles in the atmosphere; S_0 is the solar irradiance based on the ASTM G173-03 reference spectra in watts per square meters (W m^{-2}); τ_{atm}, F_c, and a_s are the atmospheric transmission (0.79), the cloud fraction (0.6), and the surface albedo (0.19), respectively, which are constants from the global average calculations; MAC with a 1 nm resolution is extrapolated using Eq. (6). And then, the fraction of solar radiation absorbed by OA component relative to BC ($f_{OA/BC}$) can be calculated as:

$$f_{OA/BC} = \frac{\sum_{\lambda=370}^{660} SFE_{OA}(\lambda) \times C_{OA}}{\sum_{\lambda=370}^{660} SFE_{BC}(\lambda) \times C_{BC}} \quad (10)$$

Here, the integrated SFE is the sum of the SFE from 370 to 660 nm; C_{OA} and C_{BC} are the average mass concentrations of OA component and BC during the sampling period.

3 Results and discussion

3.1 Overview of BrC absorption

The temporal variation in submicron aerosol b_{abs} at wavelengths from 370 to 880 nm as well as the OA mass concentration during the entire campaign at Gaomeigu are depicted in Fig. 2. The hourly b_{abs} values at different wavelengths varied from minimum to maximum values by factors of 19−41 from 14 to 31 March 2018, reflecting that atmospheric environment at Gaomeigu is influenced by dynamic changes in emission sources and meteorological condition. Particularly, the larger variations in b_{abs} values at 370−660 nm, compared with that at 880 nm, highlighted the

impact of non-BC light-absorbing materials. As shown in Table 1, the average b_{abs} values were 33.1 ± 24.4 Mm^{-1} (arithmetic mean ± standard deviation) at 370 nm, 26.7 ± 19.7 Mm^{-1} at 470 nm, 20.3 ± 13.9 Mm^{-1} at 520 nm, 18.2 ± 12.5 Mm^{-1} at 590 nm, 13.7 ± 9.0 Mm^{-1} at 660 nm, and 8.0 ± 4.9 Mm^{-1} at 880 nm. The b_{abs} values obtained in this study were comparable with those reported previously at the sampling sites of the TP, where the major anthropogenic sources (i.e., industry, fossil fuel combustion, etc.) are limited locally (Niu et al., 2018; Zhao et al., 2019; Zhu et al., 2021). Frequency histograms of hourly AAE values showed the media AAE value of 1.59 with interquartile range from 1.38 to 1.83 (Fig. S1). Over 72 % of AAE values were higher than 1.4 (Upper limit of AAE_{BC}), implying the presence of both BrC and BC absorption in the submicron aerosol at Gaomeigu.

Based on Eqs. (1) and (2), $b_{abs\text{-}BrC}$ and $b_{abs\text{-}BC}$ were separated from the total absorption using the AAE_{BC} = 1.1. The average $b_{abs\text{-}BrC}$ values during the campaign were 12.3 ± 13.8, 10.7 ± 11.5, 6.0 ± 6.0, 5.8 ± 5.8, and 2.7 ± 2.6 Mm^{-1} at 370, 470, 520, 590, and 660 nm, respectively (Table 1). Figure 3 shows fractions of light absorption at specific wavelengths by BrC and BC in the submicron aerosol. BrC contributed substantially to b_{abs}, which accounted for 20.0–40.2 % from 370 to 660 nm. The average contributions of $b_{abs\text{-}BrC}$ to b_{abs} in the near-UV and blue spectral ranges (300–500 nm) were higher than those in other visible ranges (520–880 nm), indicating that BrC was a considerable absorbing material at short wavelengths in the atmosphere. It should be noted that the assumption for AAE_{BC} would lead to the biases in the BrC absorption calculation (Lack and Langridge, 2013). The uncertainties of AAE_{BC} (± 0.3) in this study caused variations of 14.3−16.6 %, 10.2−12.2 %, 10.3−11.5 %, 7.7−8.6 %, and 6.6−7.1 % in the estimation of BrC absorption contributions at 370, 470, 520, 590, and 660 nm, respectively (Fig. 3).

With respect to the relationship between BrC absorption and OA components, $b_{abs\text{-}BrC}$ values at 370–660 nm were significantly correlated with OA mass concentrations (r = 0.64−0.70, $p < 0.01$) (Fig. S2), confirming a strong link between BrC-chromophores and OA in the southeastern margin of TP (Lack et al., 2013; Laskin et al., 2015).

3.2 OA source apportionment

HERM analysis identified two distinct OA sources, consisting of BBOA and po-OOA. Each of OA sources had unique characteristics on mass spectrum, temporary variation, and atmospheric processes. The detailed source apportionment results of OA are shown in Fig. 4.

The mass spectrum of BBOA resembled that of BBOA obtained in previous studies (Uncentered correlation coefficients = 0.80−0.87) (Crippa et al., 2013; Ng et al., 2011a; Wang et al., 2017). It was characterized by a prominent peak of *m/z* 60, and a strong positive correlation was found between BBOA and *m/z* 60 concentrations (r = 0.72, $p < 0.01$) (Figs. 4a and b). We have known that *m/z* 60 is a typical molecular fragment of levoglucosan, mannosan, and galactosan, which are good organic tracers of biomass burning (Kalogridis et al., 2018; Kim et al., 2017; Reyes-Villegas et al., 2018). The

fraction of *m/z* 60 in BBOA mass spectrum (f_{60}, 0.9 %) was higher than 0.3% (background level in absence of biomass burning), suggesting the impact of biomass burning at Gaomeigu (Cubison et al., 2011). Scatterplots of f_{44} vs. f_{60} was used to analyze aging degree of BBOA in the atmosphere (Fig. 4c). The f_{60} usually decreases from fresh to aged biomass burning emissions because of degradation and oxidation reactions during the atmospheric aging, while the f_{44} increases (Paglione et al., 2020). The f_{60} and f_{44} of BBOA resolved in this study (0.9 % and 6.3 %, respectively) indicates BBOA was less aged, possibly caused by the long-distance regional transport. This is further demonstrated in our trajectory-related analysis (Sect. 3.3).

Another OA source was featured by the high correlation with *m/z* 44 ($r = 0.97$, $p < 0.01$), which is a surrogate of oxidation degree (Aiken et al., 2008). The most abundant peak in mass spectrum of po-OOA was at *m/z* 44 (f_{44}, 27.8 %), similar to those in mass spectra of more-oxidized oxygenated OA (MO-OOA) (f_{44} > 20 %) identified frequently in previous studies (Tobler et al., 2021; Xu et al., 2018; Zhang et al., 2019). It indicated that this OA source was likely related to extensive secondary processes occurring during transport (Wang et al., 2017; Xu et al., 2017). Figure 4d shows that both po-OOA mass concentration and its fraction in OA increased with increasing O_3 ($R^2 = 0.79–0.87$), however, neither of them correlated with RH (Fig. S3). These results supported that high O_3 was the possible driving factor of po-OOA formation, thus the term of po-OOA was introduced in this study to stress the importance of photochemical-oxidation process in the TP. Moreover, the temporal variation of mass concentration in po-OOA moderately correlated with that in BBOA ($r = 0.63$, $p < 0.01$), indicating that a portion of po-OOA could be derived from oxidation of volatile organic precursor from biomass burning (Bruns et al., 2016; Posner et al., 2018).

3.3 Source-dependent characteristics of BrC absorption

To further quantify the contributions of OA sources to BrC light absorption, a MLR model was applied to retrieve MAC values from BBOA and po-OOA. As shown in Fig. 5a, the wavelength dependences of MAC_{BBOA} and $MAC_{po\text{-}OOA}$ were generally described by the power-law relationship ($R^2 = 0.84–0.87$), and the AAE of BrC values for BBOA and po-OOA were greater than 2.0 (Kirchstetter et al., 2004). The MAC_{BBOA} was 2.78 ± 0.39 $m^2\ g^{-1}$ at 370 nm, and dropped to 0.61 ± 0.07 $m^2\ g^{-1}$ at 660 nm. Taking the near-UV wavelength as the representative for discussion, the MAC_{BBOA} obtained in this study was within that range from biomass burning (0.9–7.7 $m^2\ g^{-1}$) reported by laboratory experiments and field measurements studies (Kaskaoutis et al., 2021; Kumar et al., 2018; Lack et al., 2012; Qin et al., 2018; Wang et al., 2020; Washenfelder et al., 2015). The differences in light absorption capacity of OA from biomass burning may be partly associated with biomass types and combustion efficiencies (Budisulistiorini et al., 2017; Martinsson et al., 2015; Tian et al., 2019). In addition, the photobleaching effect of aerosol at different aging degree can also lead to the variation in MAC_{BBOA} (Sumlin et al., 2017; Zhong and Jang, 2014). The $MAC_{po\text{-}OOA}$ was 1.43 ± 0.23 $m^2\ g^{-1}$ at 370 nm, 1.23 ± 0.20 $m^2\ g^{-1}$ at 470 nm, 0.68 ± 0.10 $m^2\ g^{-1}$ at 520 nm, 0.66 ± 0.10 $m^2\ g^{-1}$ at 590 nm, and 0.30 ± 0.04 $m^2\ g^{-1}$ at 660 nm. Compared

with BBOA, more oxygenated po-OOA was possibly more photochemically bleached, which resulted in the lower MAC (Lee et al., 2014).

The MLR model reasonably reconstructed the temporal variation in the measured $b_{abs\text{-}BrC}$ values, with the index of agreement ranged from 0.73 to 0.79 for different wavelengths. The total reconstructed light absorption coefficient of BrC ($rb_{abs\text{-}BrC}$) was the sum of $b_{abs\text{-}BrC}$ from BBOA and po-OOA obtained from the MLR model. As shown in Fig. 5b, the average $b_{abs\text{-}BrC}$ values from BBOA were 6.0 ± 3.6, 5.0 ± 3.0, 2.8 ± 1.7, 2.6 ± 1.6, and 1.3 ± 0.8 Mm^{-1} at 370, 470, 520, 590, and 660 nm, respectively. The $b_{abs\text{-}BrC}$ from BBOA contributed about half (48.7−51.1 %) of $rb_{abs\text{-}BrC}$ at 370−660 nm, indicating that biomass burning is an important primary source of BrC absorption at Gaomeigu. This was possibly related to transport of pollutants emitted from South and Southeast Asia during the pre-monsoon season, where biomass burning activities are intensive (Zhang et al., 2020b; Zhang et al., 2015). The po-OOA produced comparable $b_{abs\text{-}BrC}$ values (6.0 ± 4.2, 5.1 ± 3.6, 2.8 ± 2.0, 2.8 ± 1.9, and 1.3 ± 0.9 Mm^{-1} at 370, 470, 520, 590, and 660 nm, respectively), suggesting the critical role of photochemical-oxidation processes in the BrC absorption at Gaomeigu. Four periods are marked in Fig. 2, characterized by the inclusion of obvious rising stages for both OA concentrations and b_{abs} values. The $b_{abs\text{-}BrC}$ at 370 nm from BBOA contributed the most to $rb_{abs\text{-}BrC}$ (63.4 %) during the period I, while the contribution of $b_{abs\text{-}BrC}$ from po-OOA increased significantly during other periods (52.2−64.7 %) (Fig. S4). The rapid increases in $b_{abs\text{-}BrC}$ from po-OOA were likely caused by photochemical-oxidation processes that were favored by relatively high O_3 condition (75−84 ppb) during the periods II−IV; for comparison, the O_3 mixing ratio during period I was 52 ppb. We noted that the largest $rb_{abs\text{-}BrC}$ occurred in period II when both primary source emissions and secondary formation were strong. These results further highlighted the importance of biomass burning and photochemical-oxidation on light absorption of BrC at Gaomeigu.

The air-mass trajectory and CWT analyses were used to identify whether local emission or regional transported air pollution was the major source of $b_{abs\text{-}BrC}$ from OA components at Gaomeigu. Figure 6a shows the 72-h backward trajectories of the receptor site during the sampling period, and all those were originated from Myanmar. The percentage of the trajectories with high OA concentration (> 5.3 μg m^{-3}, the median value of hourly OA concentration) exceed 50%. From the CWT maps of $b_{abs\text{-}BrC}$ at 370 nm, the spatial distributions of potential source for $b_{abs\text{-}BrC}$ from BBOA and po-OOA were similar (Figs. 6b and c). The source regions with the highest CWT values were located in the northern Myanmar and along the China-Myanmar border, while the CWT values in the areas surrounding Gaomeigu were relatively low. This indicates that large $b_{abs\text{-}BrC}$ loadings at Gaomeigu were more likely resulted in strong cross-border transport of BrC from biomass burning and secondary formation than local emission during the pre-monsoon season.

3.4 Radiative effect of BrC

As described in Sect. 2.5, a simple model was used to provide a first-order estimate of the radiative effect of light-absorbing particles. Figure 7a shows SFEs of BBOA, po-OOA, and BC at wavelengths from 370 to 660 nm. The SFE peaks of BBOA, po-OOA, and BC were observed at the boundary between the UV and blue spectra (i.e., ~450 nm), that was mainly caused by the high MAC and strong solar irradiance at specific wavelength. The integrated SFE of BBOA over the entire solar spectra (370−660 nm) in this study was 24.2 W g^{-1}, comparable to that of primary OA (21 W g^{-1}, 300−1000 nm) reported in Lu et al. (2015). The integrated SFE of po-OOA (12.5 W g^{-1}) was only half of that of BBOA due to the relative lower MAC. BC had a much higher integrated SFE (226.6 W g^{-1}) compared with OAs. This is consistent with the widely acknowledged view that BC is the strongest and most important light-absorbing particle in the atmosphere (Bahadur et al., 2012; Bond et al., 2013). As the concentration of OA in the atmosphere is generally greater than that of BC, the importance of BrC radiative effect was further evaluated by calculating the fraction of solar radiation absorbed by OA relative to BC. The fractional radiative forcing by two OAs relative to BC was as high as 48.8 ± 15.5 %, in which the relative radiative forcing of po-OOA to BC (24.2 ± 13.2 %) was almost equal that of BBOA to BC (24.6 ± 9.1 %) (Fig. 7b). These results suggested that BrC emitted from biomass burning and formed by photochemical oxidation was an efficient radiative forcing agent, which, along with BC, can remarkably disturb the radiative balance over the TP. Thus, the inclusion of BrC in the climate models will provide a better understanding of climate change of the southeastern TP. It should also be noted that although BBOA and po-OOA had similar radiative effects, effective measures on tackling the impact of BrC are to reduce primary emission and volatile organic precursor of BrC from biomass burning in the future, since the intense photochemical environment is an inherent feature of the TP.

4 Conclusion

This study conducted an intensive real-time measurement at Gaomeigu in the southeastern margin of the TP during the pre-monsoon season to investigate light absorption properties, sources, secondary formation, and radiative effect of BrC in the submicron aerosol. Based on the assumption of $AAE_{BC} = 1.1$, the average $b_{abs\text{-}BrC}$ values were calculated as 12.3 ± 13.8, 10.7 ± 11.5, 6.0 ± 6.0, 5.8 ± 5.8, and 2.7 ± 2.6 Mm^{-1} at 370, 470, 520, 590, and 660 nm, respectively, which contributed 20.0–40.2 % of the total light absorption. OA was used as an alternative to BrC due to the significant correlation (r = 0.64−0.70, $p < 0.01$) between its mass concentration and $b_{abs\text{-}BrC}$. The HERM analysis identified two OA sources, including a BBOA and a po-OOA. BBOA was less aged as evidenced by the f_{60} (0.9 %) and f_{44} (6.3 %) of mass spectrum, while significant positive correlation between po-OOA and O_3 indicated that photochemical-oxidation process was possibly the main pathway for the formation of po-OOA. A MLR model combined with $b_{abs\text{-}BrC}$ and OA concentration was used to estimate the MAC of OA. The result showed that po-OOA absorbed light less efficiently

compared with BBOA due to more photobleaching effect. The MAC_{BBOA} and $MAC_{po\text{-}OOA}$ was 2.78 ± 0.39 and 1.43 ± 0.23 $m^2\ g^{-1}$ at 370 nm, and dropped to 0.61 ± 0.07 and 0.30 ± 0.04 $m^2\ g^{-1}$ at 660 nm, respectively. $b_{abs\text{-}BrC}$ from BBOA contributed about half (48.7−51.1 %) of the reconstructed $b_{abs\text{-}BrC}$ at 370−660 nm, while the rest was from po-OOA. All the 72-h backward trajectories of the Gaomeigu site came from Myanmar. The spatial distributions of potential source regions for $b_{abs\text{-}BrC}$ showed the highest CWT values for BBOA and po-OOA were both in the northern Myanmar and along the China-Myanmar border, demonstrating that biomass burning emissions and secondary formation from the cross-border transport of Southeast Asia were the major source of $b_{abs\text{-}BrC}$ at Gaomeigu. According to the integrated SFEs of BBOA, po-OOA, and BC over the solar spectra (370−660 nm) (24.2, 12.5, and 226.6 W g^{-1}, respectively), the fractional radiative forcing by BBOA (24.6 ± 9.1 %) and po-OOA (24.2 ± 13.2 %) relative to BC were obtained, highlighting the importance of BrC radiative effect. This study provides insights into light absorption properties of BrC and its potential impacts on climate change over the TP and surrounding areas.

Data availability. Data used to support the findings in this study are archived at the Institute of Earth Environment, Chinese Academy of Sciences, and are publicly available at https://doi.org/10.5281/zenodo.7496504.

Competing interests. The authors declare that they have no conflict of interest.

Author contributions. QW, YH, and JC designed the campaign. JT and JW conducted field measurements. QW, JT, and YM made data analysis and interpretation. JT wrote the paper with contributions from all co-authors.

Acknowledgments. The authors are grateful to Weikang Ran, Yonggang Zhang, and other staff at the sampling sites for their assistance with field sampling.

Financial support. This research was supported the National Natural Science Foundation of China (grant no. 41877391), the Second Tibetan Plateau Scientific Expedition and Research Program (STEP) (grant no. 2019QZKK0602), and the Youth Innovation Promotion Association of the Chinese Academy of Sciences (grant no. 2019402 and 2022416).

References

Aiken, A. C., DeCarlo, P. F., Kroll, J. H., Worsnop, D. R., Huffman, J. A., Docherty, K. S., Ulbrich, I. M., Mohr, C., Kimmel, J. R., Sueper, D., Sun, Y. L., Zhang, Q., Trimborn, A., Northway, M., Ziemann, P. J., Canagaratna, M. R., Onasch, T. B., Alfarra, M. R., Prévôt, A. S. H., Dommen, J., Duplissy, J., Metzger, A., Baltensperger, U., and Jimenez, J. L.: O/C and OM/OC ratios of primary, secondary, and ambient organic aerosols with High-Resolution Time-of-Flight Aerosol Mass Spectrometry, Environ. Sci. Technol., 42 (12), 4478−4485, https://doi.org/10.1021/es703009q, 2008.

Allan, J. D., Jimenez, J. L., Williams, P. I., Alfarra, M. R., Bower, K. N., Jayne, J. T., Coe, H., and Worsnop, D. R.: Quantitative sampling using an Aerodyne aerosol mass spectrometer – 1. Techniques of data interpretation and error analysis, J. Geophys. Res.-Atmos., 108, 4090, https://doi.org/10.1029/2002JD002358, 2003.

Andreae, M. O. and Gelencsér, A.: Black carbon or brown carbon? The nature of light-absorbing carbonaceous aerosols, Atmos. Chem. Phys., 6, 3131−3148, https://doi.org/10.5194/acp-6-3131-2006, 2006.

Bahadur, R., Praveen, P. S., Xu, Y. Y., and Ramanathan, V.: Solar absorption by elemental and brown carbon determined from spectral observations, P. Natl. Acad. Sci. USA., 109, 17366−17371, https://doi.org/ 10.1073/pnas.120591010, 2012.

Bellouin, N., Quaas, J., Morcrette, J. J., and Boucher, O.: Estimates of aerosol radiative forcing from the MACC re-analysis, Atmos. Chem. Phys., 13, 2045−2062, https://doi.org/10.5194/acp-13-2045-2013, 2013.

Bond, T. C., Doherty, S. J., Fahey, D. W., Forster, P. M., Berntsen, T., DeAngelo, B. J., Flanner, M. G., Ghan, S., Kärcher, B., Koch, D., Kinne, S., Kondo, Y., Quinn, P. K., Sarofim, M. C., Schultz, M. G., Schulz, M., Venkataraman, C., Zhang, H., Zhang, S., Bellouin, N., Guttikunda, S. K., Hopke, P. K., Jacobson, M. Z., Kaiser, J. W., Klimont, Z., Lohmann, U., Schwarz, J. P., Shindell, D., Storelvmo, T., Warren, S. G., and Zender, C. S.: Bounding the role of black carbon in the climate system: A scientific assessment, J. Geophys. Res.-Atmos., 118, 5380−5552, https://doi.org/10.1002/jgrd.50171, 2013.

Bond, T. C. and Bergstrom, R. W.: Light absorption by carbonaceous particles: An investigative review, Aerosol Sci. Tech., 40, 27−67, https://doi.org/10.1080/02786820500421521, 2006.

Brown, S. G., Eberly, S., Paatero, P., and Norris, G. A.: Methods for estimating uncertainty in PMF solutions: Examples with ambient air and water quality data and guidance on reporting PMF results, Sci. Total Environ., 518−519, 626−635, https://doi.org/10.1016/j.scitotenv.2015.01.022, 2015.

Bruns, E. A., El Haddad, I., Slowik, J. G., Kilic, D., Klein, F., Baltensperger, U., and Prévôt, A. S. H.: Identification of significant precursor gases of secondary organic aerosols from residential wood combustion, Sci. Rep-UK., 6, 27881, https://doi.org/10.1038/srep27881, 2016.

Budisulistiorini, S. H., Riva, M., Williams, M., Chen, J., Itoh, M., Surratt, J. D., and Kuwata, M.: Light-absorbing brown carbon aerosol constituents from combustion of Indonesian peat and biomass, Environ. Sci. Technol., 51, 4415−4423, https://doi.org/10.1021/acs.est.7b00397, 2017.

Chen, J. Q. and Bordoni, S.: Orographic effects of the Tibetan Plateau on the East Asian Summer Monsoon: An energetic perspective, J. Climate., 27, 3052−3072, https://doi.org/10.1175/JCLI-D-13-00479.1, 2014.

Chen, L. -W. A. and Cao, J. J.: $PM_{2.5}$ source apportionment using a hybrid environmental receptor model, Environ. Sci. Technol., 52, 6357−6369, https://doi.org/10.1021/acs.est.8b00131, 2018.

Crippa, M., DeCarlo, P. F., Slowik, J. G., Mohr, C., Heringa, M. F., Chirico, R., Poulain, L., Freutel, F., Sciare, J., Cozic, J., Di Marco, C. F., Elsasser, M., Nicolas, J. B., Marchand, N., Abidi, E., Wiedensohler, A., Drewnick, F., Schneider, J., Borrmann, S., Nemitz, E., Zimmermann, R., Jaffrezo, J. L., Prévôt, A. S. H., and Baltensperger, U.: Wintertime aerosol chemical composition and source apportionment of the organic fraction in the metropolitan area of Paris, Atmos. Chem. Phys., 13, 961−981, https://doi.org/10.5194/acp-13-961-2013, 2013.

Cubison, M. J., Ortega, A. M., Hayes, P. L., Farmer, D. K., Day, D., Lechner, M. J., Brune, W. H., Apel, E., Diskin, G. S., Fisher, J. A., Fuelberg, H. E., Hecobian, A., Knapp, D. J., Mikoviny, T., Riemer, D., Sachse, G. W., Sessions, W., Weber, R. J., Weinheimer, A. J., and Jimenez, J. L.: Effects of aging on organic aerosol from open biomass burning smoke in aircraft and laboratory studies, Atmos. Chem. Phys., 11, 12049−12064, https://doi.org/10.5194/acp-11-12049-2011, 2011.

Draxler, R. R. and Hess, G. D.: An overview of the HYSPLIT_4 modelling system for trajectories, dispersion, and deposition, Aust. Met. Mag., 47, 295−308, 1998.

Drinovec, L., Močnik, G., Zotter, P., Prévôt, A. S. H., Ruckstuhl, C., Coz, E., Rupakheti, M., Sciare, J., Müller, T., Wiedensohler, A., and Hansen, A. D. A.: The "dual-spot" Aethalometer: an improved measurement of aerosol black carbon with real-time loading compensation, Atmos. Meas. Tech., 8, 1965−1979, https://doi.org/10.5194/amt-8-1965-2015, 2015.

Du, W., Sun, Y. L., Xu, Y. S., Jiang, Q., Wang, Q. Q., Wang, W., Wang, F., Bai, Z. P., Zhao, X. D., and Yang, Y. C.: Chemical characterization of submicron aerosol and particle growth events at a national background site (3295 m a.s.l.) on the Tibetan Plateau, Atmos. Chem. Phys., 15, 10811−10824, https://doi.org/10.5194/acp-15-10811-2015, 2015.

Duan, J., Huang, R. J., Gu, Y. F., Lin, C. S., Zhong, H. B., Xu, W., Liu, Q., You, Y., Ovadnevaite, J., Ceburnis, D., Hoffmann, T., and O'Dowd, C.: Measurement report: Large contribution of biomass burning and aqueous-phase processes to the wintertime secondary organic aerosol formation in Xi'an, Northwest China, Atmos. Chem. Phys., 22, 10139−10153, https://doi.org/10.5194/acp-22-10139-2022, 2022.

Feng, Y., Ramanathan, V., and Kotamarthi, V. R.: Brown carbon: a significant atmospheric absorber of solar radiation? Atmos. Chem. Phys., 13, 8607−8621, https://doi.org/10.5194/acp-13-8607-2013, 2013.

Florou, K., Papanastasiou, D. K., Pikridas, M., Kaltsonoudis, C., Louvaris, E., Gkatzelis, G. I., Patoulias, D., Mihalopoulos, N., and Pandis, S. N.: The contribution of wood burning and other pollution sources to wintertime organic aerosol levels in two Greek cities, Atmos. Chem. Phys., 17, 3145−3163, https://doi.org/10.5194/acp-17-3145-2017, 2017.

Hecobian, A., Zhang, X., Zheng, M., Frank, N., Edgerton, E. S., and Weber, R. J.: Water-Soluble Organic Aerosol material and the light-absorption characteristics of aqueous extracts measured over the Southeastern United States, Atmos. Chem. Phys., 10, 5965−5977, https://doi.org/10.5194/acp-10-5965-2010, 2010.

Hsu, Y. K., Holsen, T. M., and Hopke, P. K.: Comparison of hybrid receptor models to locate PCB sources in Chicago, Atmos. Environ., 37, 545−562, https://doi.org/10.1016/S1352-2310(02)00886-5, 2003.

Huang, R. J., Wang, Y. C., Cao, J. J., Lin, C. S., Duan, J., Chen, Q., Li, Y. J., Gu, Y. F., Yan, J., Xu, W., Fröhlich, R., Canonaco, F., Bozzetti, C., Ovadnevaite, J., Ceburnis, D., Canagaratna, M. R., Jayne, J., Worsnop, D. R., El-Haddad, I., Prévôt, A. S. H., and O'Dowd, C. D.: Primary emissions versus secondary formation of fine particulate matter in the most polluted city (Shijiazhuang) in North China, Atmos. Chem. Phys., 19, 2283−2298, https://doi.org/10.5194/acp-19-2283-2019, 2019.

Immerzeel, W. W., van Beek, L. P. H., and Bierkens, M. F. P.: Climate change will affect the Asian water towers, Science, 328, 1382−1385, https://doi.org/10.1126/science.1183188, 2010.

IPCC: Climate change 2013: The physical science basis. Contribution of working group I to the fifth assessment report of the intergovernmental panel on climate change, edited by: Stocker, T. F., Qin, D., Plattner, G. -K., Tignor, M., Allen, S. K., Boschung, J., Nauels, A., Xia, Y., Bex, V., and Midgley, P.M., Cambridge University Press, Cambridge, United Kingdom and New York, NY, USA, 1535 pp., ISBN 978-1-107-66182-0, 2013.

Kalogridis, A. C., Popovicheva, O. B., Engling, G., Diapouli, E., Kawamura, K., Tachibana, E., Ono, K., Kozlov, V. S., and Eleftheriadis, K.: Smoke aerosol chemistry and aging of Siberian biomass burning emissions in a large aerosol chamber, Atmos. Environ., 185, 15−28, https://doi.org/10.1016/j.atmosenv.2018.04.033, 2018.

Kaskaoutis, D. G., Grivas, G., Stavroulas, I., Bougiatioti, A., Liakakou, E., Dumka, U. C., Gerasopoulos, E., and Mihalopoulos, N.: Apportionment of black and brown carbon spectral absorption sources in the urban environment of Athens, Greece, during winter, Sci. Total Environ., 801, 149739, https://doi.org/10.1016/j.scitotenv.2021.149739, 2021.

Kehrwald, N. M., Thompson, L. G., Yao, T. D., Mosley-Thompson, E., Schotterer, U., Alfimov, V., Beer, J., Eikenberg, J., and Davis, M. E.: Mass loss on Himalayan glacier endangers water resources, Geophys. Res. Lett., 35, L22503, https://doi.org/10.1029/2008GL035556, 2008.

Kim, H., Zhang, Q., Bae, G. N., Kim, J. Y., and Lee, S. B.: Sources and atmospheric processing of winter aerosols in Seoul, Korea: Insights from real-time measurements using a high-resolution aerosol mass spectrometer, Atmos. Chem. Phys., 17, 2009−2033, https://doi.org/10.5194/acp-17-2009-2017, 2017.

Kirchstetter, T. W., Novakov, T., and Hobbs, P. V.: Evidence that the spectral dependence of light absorption by aerosols is affected by organic carbon, J. Geophys. Res., 109, D21208, https://doi.org/10.1029/2004JD004999, 2004.

Koch, D., Bond, T. C., Streets, D., Unger, N., and van der Werf, G. R.: Global impacts of aerosols from particular source regions and sectors, J. Geophys. Res.-Atmos., 112, D02205, https://doi.org/10.1029/2005JD007024, 2007.

Kopacz, M., Mauzerall, D. L., Wang, J., Leibensperger, E. M., Henze, D. K., and Singh, K., 2011. Origin and radiative forcing of black carbon transported to the Himalayas and Tibetan Plateau, Atmos. Chem. Phys., 11, 2837−2852, https://doi.org/10.5194/acp-11-2837-2011, 2011.

Kumar, N. K., Corbin, J. C., Bruns, E. A., Massabó, D., Slowik, J. G., Drinovec, L., Močnik, G., Prati, P., Vlachou, A., Baltensperger, U., Gysel, M., El-Haddad, I., and Prévt, A. S. H.: Production of particulate brown carbon during atmospheric aging of residential wood-burning emissions, Atmos. Chem. Phys., 18, 17843−17861, https://doi.org/10.5194/acp-18-17843-2018, 2018.

Lack, D. A. and Langridge, J. M.: On the attribution of black and brown carbon light absorption using the Ångström exponent, Atmos. Chem. Phys., 13, 10535−10543, https://doi.org/10.5194/acp-13-10535-2013, 2013.

Lack, D. A. and Cappa, C. D.: Impact of brown and clear carbon on light absorption enhancement, single scatter albedo and absorption wavelength dependence of black carbon, Atmos. Chem. Phys., 10, 4207−4220, https://doi.org/10.5194/acp-10-4207-2010, 2010.

Lack, D. A., Bahreini, R., Langridge, J. M., Gilman, J. B., and Middlebrook, A. M.: Brown carbon absorption linked to organic mass tracers in biomass burning particles, Atmos. Chem. Phys., 13, 2415−2422, https://doi.org/10.5194/acp-13-2415-2013, 2013.

Lack, D. A., Langridge, J. M., Bahreini, R., Cappa, C. D., Middlebrook, A. M., and Schwarz, J. P.: Brown carbon and internal mixing in biomass burning particles, P. Natl. Acad. Sci. USA., 109, 14802−14807, https://doi.org/10.1073/pnas.120657510, 2012.

Laskin, A., Laskin, J., and Nizkorodov, S. A.: Chemistry of atmospheric brown carbon, Chem. Rev., 115, 4335−4382, https://doi.org/10.1021/cr5006167, 2015.

Lau, W. K. M., Kim, M. -K., Kim, K. -M., and Lee, W. -S.: Enhanced surface warming and accelerated snow melt in the Himalayas and Tibetan Plateau induced by absorbing aerosols, Environ. Res. Lett., 5, 025204, https://doi.org/10.1088/1748-9326/5/2/025204, 2010.

Lee, H. J., Aiona, P. K., Laskin, A., Laskin, J., and Nizkorodov, S. A.: Effect of solar radiation on the optical properties and molecular composition of laboratory proxies of atmospheric brown carbon, Environ. Sci. Technol., 48(17), 10217−10226, https://doi.org/10.1021/es502515r, 2014.

Lin, G. X., Penner, J. E., Flanner, M. G., Sillman, S., Xu, L., and Zhou, C.: Radiative forcing of organic aerosol in the atmosphere and on snow: Effects of SOA and brown carbon, J. Geophys. Res.-Atmos., 119, 7453−7476, https://doi.org/10.1002/2013JD021186, 2014.

Liu, H. K., Wang, Q. Y., Xing, L., Zhang, Y., Zhang, T., Ran, W. K., and Cao, J. J.: Measurement report: quantifying source contribution of fossil fuels and biomass-burning black carbon aerosol in the southeastern margin of the Tibetan Plateau, Atmos. Chem. Phys., 21, 973−987, https://doi.org/10.5194/acp-21-973-2021, 2021.

Liu, X. D. and Chen, B. D.: Climatic warming in the Tibetan Plateau during recent decades, Int. J. Climatol., 20, 1729−1742, https://doi.org/10.1002/1097-0088(20001130)20:14<1729::AID-JOC556>3.0.CO;2-Y, 2000.

Martinsson, J., Eriksson, A. C., Nielsen, I. E., Malmborg, V. B., Ahlberg, E., Andersen, C., Lindgren, R., Nyström, R., Nordin, E. Z., Brune, W. H., Svenningsson, B., Swietlicki, E., Boman, C., and Pagels, J. H.: Impacts of combustion conditions and photochemical processing on the light absorption of biomass combustion aerosol, Environ. Sci. Technol., 49, 14663−14671, https://doi.org/10.1021/acs.est.5b03205, 2015.

Middlebrook, A. M., Bahreini, R., Jimenez, J. L., and Canagaratna, M. R.: Evaluation of composition-dependent collection efficiencies for the aerodyne aerosol mass spectrometer using field data, Aerosol Sci. Tech., 46, 258−271, https://doi.org/10.1080/02786826.2011.620041, 2012.

Moschos, V., Kumar, N. K., Daellenbach, K. R., Baltensperger, U., Prévôt, A. S. H., and El Haddad, I.: Source apportionment of brown carbon absorption by coupling UV/Vis spectroscopy with aerosol mass spectrometry, Environ. Sci. Technol. Lett., 5, 302−308, https://doi.org/10.1021/acs.estlett.8b00118, 2018.

Nakayama, T., Sato, K., Matsumi, Y., Imamura, T., Yamazaki, A., and Uchiyama, A.: Wavelength and NO_x dependent complex refractive index of SOAs generated from the photooxidation of toluene, Atmos. Chem. Phys., 13, 531−545, https://doi.org/10.5194/acp-13-531-2013, 2013.

Ng, N. L., Canagaratna, M. R., Jimenez, J. L., Zhang, Q., Ulbrich, I. M., and Worsnop, D. R.: Real-time methods for estimating organic component mass concentrations from aerosol mass spectrometer data, Environ. Sci. Technol., 45, 910−916, https://doi.org/10.1021/es102951k, 2011a.

Ng, N. L., Herndon, S. C., Trimborn, A., Canagaratna, M. R., Croteau, P. L., Onasch, T. B., Sueper, D., Worsnop, D. R., Zhang, Q., Sun, Y. L., and Jayne, J. T.: An aerosol chemical speciation monitor (ACSM) for routine monitoring of the composition and mass concentrations of ambient aerosol, Aerosol Sci. Tech., 45, 780−794, https://doi.org/10.1080/02786826.2011.560211, 2011b.

Niu, H. W., Kang, S. C., Wang, H. L., Zhang, R. D., Lu, X. X., Qian, Y., Paudyal, R., Wang, S. J., Shi, X. F., and Yan, X. G.: Seasonal variation and light absorption property of carbonaceous aerosol in a typical glacier region of the southeastern Tibetan Plateau, Atmos. Chem. Phys., 18, 6441−6460, https://doi.org/10.5194/acp-18-6441-2018, 2018.

Olson, M. R., Garcia, M. V., Robinson, M. A., Rooy, P. V., Dietenberger, M. A., Bergin, M., and Schauer, J. J.: Investigation of black and brown carbon multiple-wavelength-dependent light absorption from biomass and fossil fuel combustion source emissions, J. Geophys. Res.-Atmos., 120, 6682−6697, https://doi.org/10.1002/2014JD022970, 2015.

Paglione, M., Gilardoni, S., Rinaldi, M., Decesari, S., Zanca, N., Sandrini, S., Giulianelli, L., Bacco, D., Ferrari, S., Poluzzi, V., Scotto, F., Trentini, A., Poulain, L., Herrmann, H., Wiedensohler, A., Canonaco, F., Prévôt, A. S. H., Massoli, P., Carbone, C., Facchini, M. C., and Fuzzi, S.: The impact of biomass burning and aqueous-phase processing on air quality: a multi-year source apportionment study in the Po Valley, Italy, Atmos. Chem. Phys., 20, 1233−1254, https://doi.org/10.5194/acp-20-1233-2020, 2020.

Panicker, A. S., Sandeep, K., Gautam, A. S., Trimbake, H. K., Nainwal, H. C., Beig, G., Bisht, D. S., and Das, S.: Black carbon over a central Himalayan Glacier (Satopanth): Pathways and direct radiative impacts, Sci. Total Environ., 766, 144242, https://doi.org/10.1016/j.scitotenv.2020.144242, 2020.

Pokhrel, R. P., Beamesderfer, E. R., Wagner, N. L., Langridge, J. M., Lack, D. A., Jayarathne, T., Stone, E. A., Stockwell, C. E., Yokelson, R. J., and Murphy, S. M.: Relative importance of black carbon, brown carbon and absorption enhancement from clear coatings in biomass burning emissions, Atmos. Chem. Phys., 17, 5063−5078, https://doi.org/10.5194/acp-17-5063-2017, 2017.

Posner, L. N., Theodoritsi, G., Robinson, A., Yarwood, G., Koo, B., Morris, R., Mavko, M., Moore, T., and Pandis, S. N.: Simulation of fresh and chemically-aged biomass burning organic aerosol. Atmos. Environ. 196, 27−37. https://doi.org/10.1016/j.atmosenv.2018.09.055, 2018.

Qian, Y., Flanner, M. G., Leung, L. R., and Wang, W.: Sensitivity studies on the impacts of Tibetan Plateau snowpack pollution on the Asian hydrological cycle and monsoon climate, Atmos. Chem. Phys., 11, 1929−1948, https://doi.org/10.5194/acp-11-1929-2011, 2011.

Qin, Y. M., Tan, H. B., Li, Y. J., Li, Z. J., Schurman, M. I., Liu, L., Wu, C., and Chan, C. K.: Chemical characteristics of brown carbon in atmospheric particles at a suburban site near Guangzhou, China, Atmos. Chem. Phys., 18, 16409−16418, https://doi.org/10.5194/acp-18-16409-2018, 2018.

Ramanathan, V., Ramana, M. V., Roberts, G., Kim, D., Corrigan, C., Chung, C., and Winker, D.: Warming trends in Asia amplified by brown cloud solar absorption, Nature, 448, 575−578, https://doi.org/10.1038/nature06019, 2007.

Reyes-Villegas, E., Priestley, M., Ting, Y. C., Haslett, S., Bannan, T., Le Breton, M., Williams, P. I., Bacak, A., Flynn, M. J., Coe, H., Percival, C., and Allan, J. D.: Simultaneous aerosol mass spectrometry and chemical ionisation mass spectrometry measurements during a biomass burning event in the UK: Insights into nitrate chemistry, Atmos. Chem. Phys., 18, 4093−4111, https://doi.org/10.5194/acp-18-4093-2018, 2018.

Sumlin, B. J., Pandey, A., Walker, M. J., Pattison, R. S., Williams, B. J., and Chakrabarty, R. K.: Atmospheric photooxidation diminishes light absorption by primary brown carbon aerosol from biomass burning, Environ. Sci. Technol. Lett., 4, 540−545, https://doi.org/10.1021/acs.estlett.7b00393, 2017.

Tan, T. Y., Hu, M., Du, Z. F., Zhao, G., Shang, D. J., Zheng, J., Qin, Y. H., Li, M. R., Wu, Y. S., Zeng, L. M., Guo, S., and Wu, Z. J.: Measurement report: Strong light absorption induced by aged biomass burning black carbon over the southeastern Tibetan Plateau in pre-monsoon season, Atmos. Chem. Phys., 21, 8499−8510, https://doi.org/10.5194/acp-21-8499-2021, 2021.

Tian, J., Wang, Q. Y., Ni, H. Y., Wang, M., Zhou, Y. Q., Han, Y. M., Shen, Z. X., Pongpiachan, S., Zhang, N. N., Zhao, Z. Z., Zhang, Q., Zhang, Y., Long, X., and Cao, J. J.: Emission characteristics of primary brown carbon absorption from biomass and coal burning: Development of an optical emission inventory for China, J. Geophys. Res.-Atmos., 124, 1879−1893, https://doi.org/10.1029/2018jd029352, 2019.

Tian, J., Wang, Q. Y., Zhang, Y., Yan, M. Y., Liu, H. K., Zhang, N. N., Ran, W. K., and Cao, J. J.: Impacts of primary emissions and secondary aerosol formation on air pollution in an urban area of China during the COVID-19 lockdown, Environ. Int., 150, 106426, https://doi.org/10.1016/j.envint.2021.106426, 2021.

Tobler, A. K., Skiba, A., Canonaco, F., Močnik, G., Rai, P., Chen, G., Bartyzel, J., Zimnoch, M., Styszko, K., Nęcki, J., Furger, M., Różański, K., Baltensperger, U., Slowik, J. G., and Prevot, A. S. H.: Characterization of non-refractory (NR) PM_1 and source apportionment of organic aerosol in Kraków, Poland, Atmos. Chem. Phys., 21, 14893−14906, https://doi.org/10.5194/acp-21-14893-2021, 2021.

Ulbrich, I. M., Canagaratna, M. R., Zhang, Q., Worsnop, D. R., and Jimenez, J. L.: Interpretation of organic components from Positive Matrix Factorization of aerosol mass spectrometric data, Atmos. Chem. Phys., 9, 2891−2918, https://doi.org/10.5194/acp-9-2891-2009, 2009.

Wang, B., Bao, Q., Hoskins, B., Wu, G. X., and Liu, Y. M.: Tibetan Plateau warming and precipitation changes in East Asia, Geophys. Res. Lett., 35, L14702, https://doi.org/10.1029/2008GL034330, 2008.

Wang, J. F., Ye, J. H., Zhang, Q., Zhao, J., Wu, Y. Z., Li, J. Y., Liu, D. T., Li, W. J., Zhang, Y. G., Wu, C., Xie, C. H., Qin, Y. M., Lei, Y. L., Huang, X. P., Guo, J. P., Liu, P. F., Fu, P. Q., Li, Y. J., Lee, H. C., Choi, H., Zhang, J., Liao, H., Chen, M. D., Sun, Y. L., Ge, X. L., Martin, S. T., and Jacob, D. J.: Aqueous production of secondary organic

aerosol from fossil-fuel emissions in winter Beijing haze, P. Natl. Acad. Sci. USA., 118, e2022179118, https://doi.org/10.1073/pnas.2022179118, 2021.

Wang, Q. Y., Han, Y. M., Ye, J. H., Liu, S. X., Pongpiachan, S., Zhang, N. N., Han, Y. M., Tian, J., Wu, C., Long, X., Zhang, Q., Zhang, W. Y., Zhao, Z. Z., and Cao, J. J.: High contribution of secondary brown carbon to aerosol light absorption in the southerastern margin of Tibetan Plateau, Geophys. Res. Lett., 46, 4962−4970, https://doi.org/10.1029/2019GL082731, 2019.

Wang, Q. Y., Liu, H. K., Wang, P., Dai, W. T., Zhang, T., Zhao, Y. Z., Tian, J., Zhang, W. Y., Han, Y. M., and Cao, J. J.: Optical source apportionment and radiative effect of light-absorbing carbonaceous aerosols in a tropical marine monsoon climate zone: the importance of ship emissions, Atmos. Chem. Phys., 20, 15537−15549, https://doi.org/10.5194/acp-20-15537-2020, 2020.

Wang, Y. C., Huang, R. J., Ni, H. Y., Chen, Y., Wang, Q. Y., Li, G. H., Tie, X. X., Shen, Z. X., Huang, Y., Liu, S. X., Dong, W. M., Xue, P., Fröhlich, R., Canonaco, F., Elser, M., Daellenbach, K. R., Bozzetti, C., El Haddad, I., Prévôt, A. S. H., Canagaratna, M. R., Worsnop, D. R., and Cao, J. J.: Chemical composition, sources and secondary processes of aerosols in Baoji city of northwest China, Atmos. Environ., 158, 128−137, https://doi.org/10.1016/j.atmosenv.2017.03.026, 2017.

Wang, Y. Q., Zhang, X. Y., and Arimoto, R.: The contribution from distant dust sources to the atmospheric particulate matter loadings at XiAn, China during spring, Sci. Total Environ., 368, 875−883, https://doi.org/10.1016/j.scitotenv.2006.03.040, 2006.

Wang, Y. Q., Zhang, X. Y., and Draxler, R. R.: TrajStat: GIS-based software that uses various trajectory statistical analysis methods to identify potential sources from long-term air pollution measurement data, Environ. Modell. Softw., 24, 938−939, https://doi.org/10.1016/j.envsoft.2009.01.004, 2009.

Washenfelder, R. A., Attwood, A. R., Brock, C. A., Guo, H., Xu, L., Weber, R. J., Ng, N. L., Allen, H. M., Ayres, B. R., Baumann, K., Cohen, R. C., Draper, D. C., Duffey, K. C., Edgerton, E., Fry, J. L., Hu, W. W., Jimenez, J. L., Palm, B. B., Romer, P., Stone, E. A., Wooldridge, P. J., and Brown, S. S.: Biomass burning dominates brown carbon absorption in the rural southeastern United States, Geophys. Res. Lett., 42, 653−664, https://doi.org/10.1002/2014GL062444, 2015.

Weingartner, E., Saathoff, H., Schnaiter, M., Streit, N., Bitnar, B., and Baltensperger, U.: Absorption of light by soot particles: determination of the absorption coefficient by means of aethalometers, J. Aerosol Sci., 34, 1445−1463, https://doi.org/10.1016/S0021-8502(03)00359-8, 2003.

Xie, M. J., Hays, M. D., and Holder, A. L.: Light-absorbing organic carbon from prescribed and laboratory biomass burning and gasoline vehicle emissions, Sci. Rep-UK., 7, 7318, https://doi.org/10.1038/s41598-017-06981-8, 2017.

Xu, J. Z., Zhang, Q., Shi, J. S., Ge, X. L., Xie, C. H., Wang, J. F., Kang, S. C., Zhang, R. X., and Wang, Y. H.: Chemical characteristics of submicron particles at the central Tibetan Plateau: insights from aerosol mass spectrometry, Atmos. Chem. Phys., 18, 427−443, https://doi.org/10.5194/acp-18-427-2018, 2018.

Xu, W. Q., Han, T. T., Du, W., Wang, Q. Q., Chen, C., Zhao, J., Zhang, Y. J., Li, J., Fu, P. Q., Wang, Z. F., Worsnop, D. R., and Sun, Y. L.: Effects of aqueous-phase and photochemical processing on secondary organic aerosol formation and evolution in Beijing, China, Environ. Sci. Technol., 51, 762−770, https://doi.org/10.1021/acs.est.6b04498, 2017.

Yao, T. D., Thompson, L. G., Mosbrugger, V., Zhang, F., Ma, Y. M., Luo, T. X., Xu, B. Q., Yang, X. X., Joswiak, D. R., Wang, W. C., Joswiak, M. E., Devkota, L. P., Tayal, S., Jilani, R., and Fayziev, R.: Third Pole Environment (TPE), Environ. Dev., 3, 52−64, http://doi.org/10.1016/j.envdev.2012.04.002, 2012.

Yao, H., Song, Y., Liu, M. X., Archer-Nicholls, S., Lowe, D., McFiggans, G., Xu, T. T., Du, P., Li, J. F., Wu, Y. S., Hu, M., Zhao, C., and Zhu, T.: Direct radiative effect of carbonaceous aerosols from crop residue burning during the summer harvest season in East China, Atmos. Chem. Phys., 17, 5205−5219, https://doi.org/10.5194/acp-17-5205-2017, 2017.

Zhang, A. X., Wang, Y. H., Zhang, Y. Z., Weber, R. J., Song, Y. J., Ke, Z. M., and Zou, Y. F.: Modeling global radiative effect of brown carbon: A larger heating source in the tropical free troposphere than black carbon, Atmos. Chem. Phys., 20(4), 1901−1920, https://doi.org/10.5194/acp-20-1901-2020, 2020a.

Zhang, M. X., Zhao, C., Cong, Z. Y., Du, Q. Y., Xu, M. Y., Chen, Y., Chen, M., Li, R., Fu, Y. F., Lei, Z., Kang, S. C., Zhao, D. L., and Yang, Y.: Impact of topography on black carbon transport to the southern Tibetan Plateau during the pre-monsoon season and its climatic implication, Atmos. Chem. Phys., 20, 5923−5943, https://doi.org/10.5194/acp-20-5923-2020, 2020b.

Zhang, R., Wang, H., Qian, Y., Rasch, P. J., Easter, R. C., Ma, P. L., Singh, B., Huang, J., and Fu, Q.: Quantifying sources, transport, deposition, and radiative forcing of black carbon over the Himalayas and Tibetan Plateau, Atmos. Chem. Phys., 15, 6205−6223, https://doi.org/10.5194/acp-15-6205-2015, 2015.

Zhang, X. H., Xu, J. Z., Kang, S. C., Zhang, Q., and Sun, J. Y.: Chemical characterization and sources of submicron aerosols in the northeastern Qinghai–Tibet Plateau: insights from high-resolution mass spectrometry, Atmos. Chem. Phys., 19, 7897−7911, https://doi.org/10.5194/acp-19-7897-2019, 2019.

Zhang, Y. Z., Forrister, H., Liu, J. M., Dibb, J., Anderson, B., Schwarz, J. P., Perring, A. E., Jimenez, J. L., Campuzano-Jost, P., and Wang, Y. H.: Top-of-atmosphere radiative forcing affected by brown carbon in the upper troposphere, Nat. Geosci., 10, 486−489, https://doi.org/10.1038/NGEO2960, 2017.

Zhao, Z. Z., Cao, J. J., Chow, J. C., Watson, J. G., Chen, L. -W. A., Wang, X. L., Wang, Q. Y., Tian, J., Shen, Z. X., Zhu, C. S., Liu, S. X., Tao, J., Ye, Z. L., Zhang, T., Zhou, J. M., and Tian, R. X.: Multi-wavelength light absorption of black and brown carbon at a high-altitude site on the Southeastern margin of the Tibetan Plateau, China, Atmos. Environ., 212, 54−64, https://doi.org/10.1016/j.atmosenv.2019.05.035, 2019.

Zhong, M. and Jang, M.: Dynamic light absorption of biomass-burning organic carbon photochemically aged under natural sunlight, Atmos. Chem. Phys., 14, 1517−1525, https://doi.org/10.5194/acp-14-1517-2014, 2014.

Zhu, C. S., Qu, Y., Huang, H., Chen, J., Dai, W. T., Huang, R. J., and Cao, J. J.: Black carbon and secondary brown carbon, the dominant light absorption and direct radiative forcing contributors of the atmospheric aerosols over the Tibetan Plateau, Geophys. Res. Lett., 48, e2021GL092524, https://doi.org/ 10.1029/2021GL092524, 2021.

Table 1. Submicron aerosol light absorption coefficient (b_{abs}) contributed by BrC ($b_{abs\text{-}BrC}$) and BC ($b_{abs\text{-}BC}$) at Gaomeigu during the sampling period (March 14th to 31th, 2018).

Parameter* (Mm^{-1})	Wavelength					
	370 nm	470 nm	520 nm	590 nm	660 nm	880 nm
b_{abs}	33.1 ±24.4 (4.7−160.0)**	26.7 ±19.7 (3.8−138.4)	20.3 ±13.9 (2.6−93.0)	18.2 ±12.5 (2.1−84.8)	13.7 ±9.0 (1.7−56.9)	8.0 ±4.9 (1.5−28.6)
$b_{abs\text{-}BrC}$	12.3 ±13.8	10.7 ±11.5	6.0 ±6.0	5.8 ±5.8	2.7 ±2.6	0.0 ±0.0
$b_{abs\text{-}BC}$	20.8 ±12.8	16.0 ±9.8	14.3 ±8.8	12.4 ±7.7	11.0 ±6.8	8.0 ±4.9

*$b_{abs\text{-}BrC}$ and $b_{abs\text{-}BC}$ were calculated based on the AAE_{BC} = 1.1.

**The measured hourly b_{abs} from minimum to maximum values.

Figure captions:

Figure 1. Topography map of the Tibetan Plateau and the location of the sampling site at Gaomeigu.

Figure 2. Hourly variations in (a) OA mass concentrations and (b) submicron aerosol light absorption coefficients (b_{abs}) at different wavelengths (370, 470, 520, 590, 660 and 880 nm) at Gaomeigu from 14 to 31 March, 2018.

Figure 3. Light absorption fractions at specific wavelengths contributed by BrC and BC under different absorption Ångström exponent of BC (AAE_{BC}) assumptions. The red, blue, and green lines were the dividing lines between BrC and BC light absorption fractions when AAE_{BC} = 1.1, 0.8, and 1.4, respectively. The grey filled area represents variations in the BrC absorption fraction caused by the uncertainties of AAE_{BC} ($\pm$0.3).

Figure 4. (a) Mass spectra of BBOA and po-OOA. (b) Pearson correlations between mass concentrations of OA components and the tracer molecular fragments. (c) Scatterplots of f_{44} vs. f_{60} for BBOA resolved in this study and reported by previous literatures. (d) Variations of po-OOA mass concentration and its fraction in OA as a function of O_3. The data are grouped in O_3 bins (10 ppb increment).

Figure 5. (a) The mass absorption cross section of BBOA and po-OOA (MAC_{BBOA} and $MAC_{po\text{-}OOA}$, respectively) at five wavelengths (λ = 370, 470, 520, 590, and 660 nm). The circle and shaded area represent the mean MAC values and the standard deviations, respectively. The dashed line is power-law fit. (b) Light absorption coefficient of BrC ($b_{abs\text{-}BrC}$) from BBOA and po-OOA and its fraction in the total reconstructed BrC absorption at different wavelengths.

Figure 6. (a) 72-h backward trajectories of Gaomeigu from 8:00 on 14 to 23:00 on 31 March, 2018. (b) and (c) Concentration weighted trajectory (CWT) maps of $b_{abs\text{-}BrC}$ at 370 nm (Mm^{-1}) from BBOA and po-OOA, respectively.

Figure 7. (a) Simple forcing efficiency (SFE) of light-absorbing particles from 370 to 660 nm and the integrated SFE over the entire solar spectra (370−660 nm). (b) The fraction of solar radiation absorbed by OA components relative to BC. In each panel, the short line and square inside the boxes indicate the median and mean values, respectively. The lower and upper edges of the boxes denote the standard deviation. The vertical bars ("whiskers") show the 5^{th} and 95^{th} percentiles. Scattered data points and normal distribution curve are also shown.

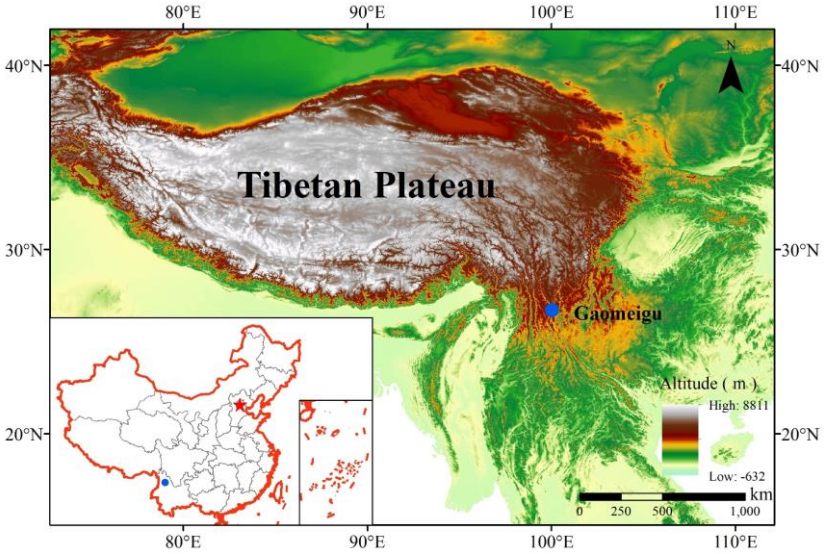

Figure 1. Topography map of the Tibetan Plateau and the location of the sampling site at Gaomeigu.

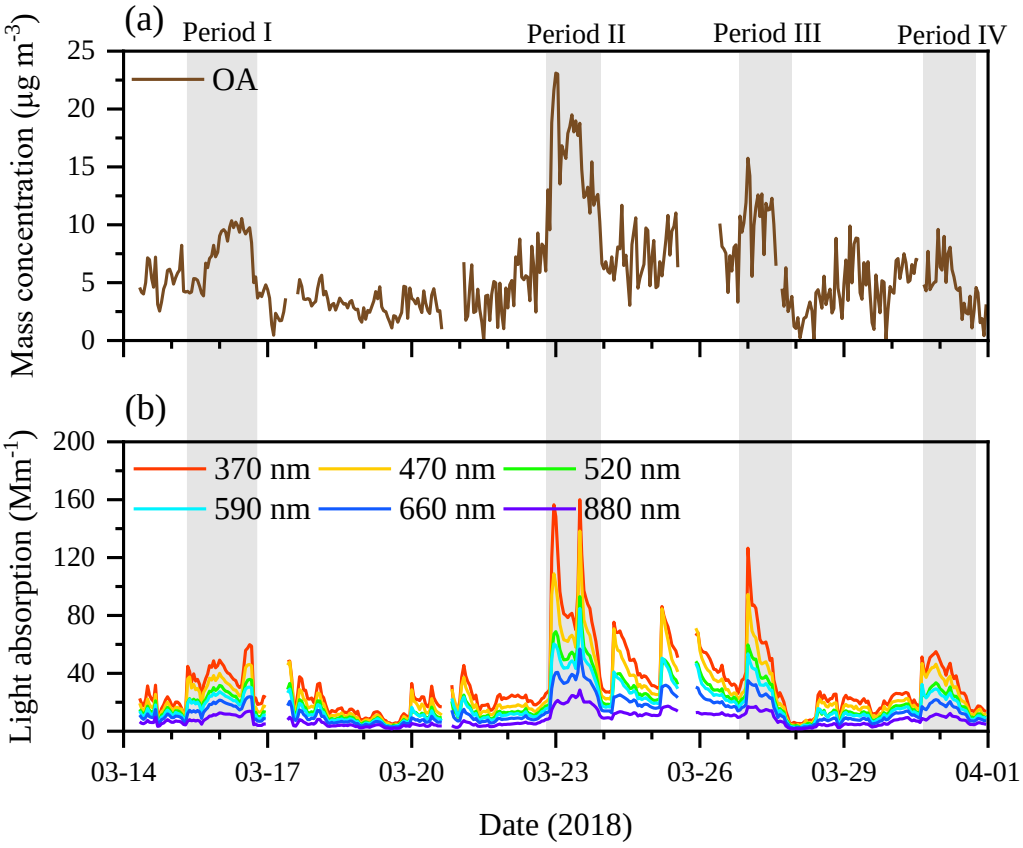

Figure 2. Hourly variations in (a) OA mass concentrations and (b) submicron aerosol light absorption coefficients (b_{abs}) at different wavelengths (370, 470, 520, 590, 660 and 880 nm) at Gaomeigu from 14 to 31 March, 2018.

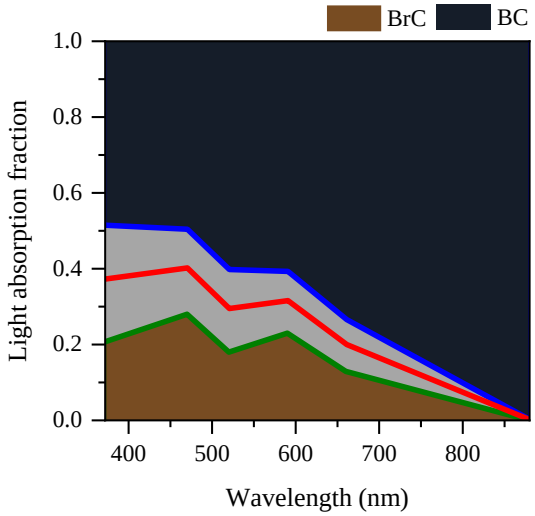

660

Figure 3. Light absorption fractions at specific wavelengths contributed by BrC and BC under different absorption Ångström exponent of BC (AAE_{BC}) assumptions. The red, blue, and green lines were the dividing lines between BrC and BC light absorption fractions when AAE_{BC} = 1.1, 0.8, and 1.4, respectively. The grey filled area represents variations in the BrC absorption fraction caused by the uncertainties of AAE_{BC} ($\pm$0.3).

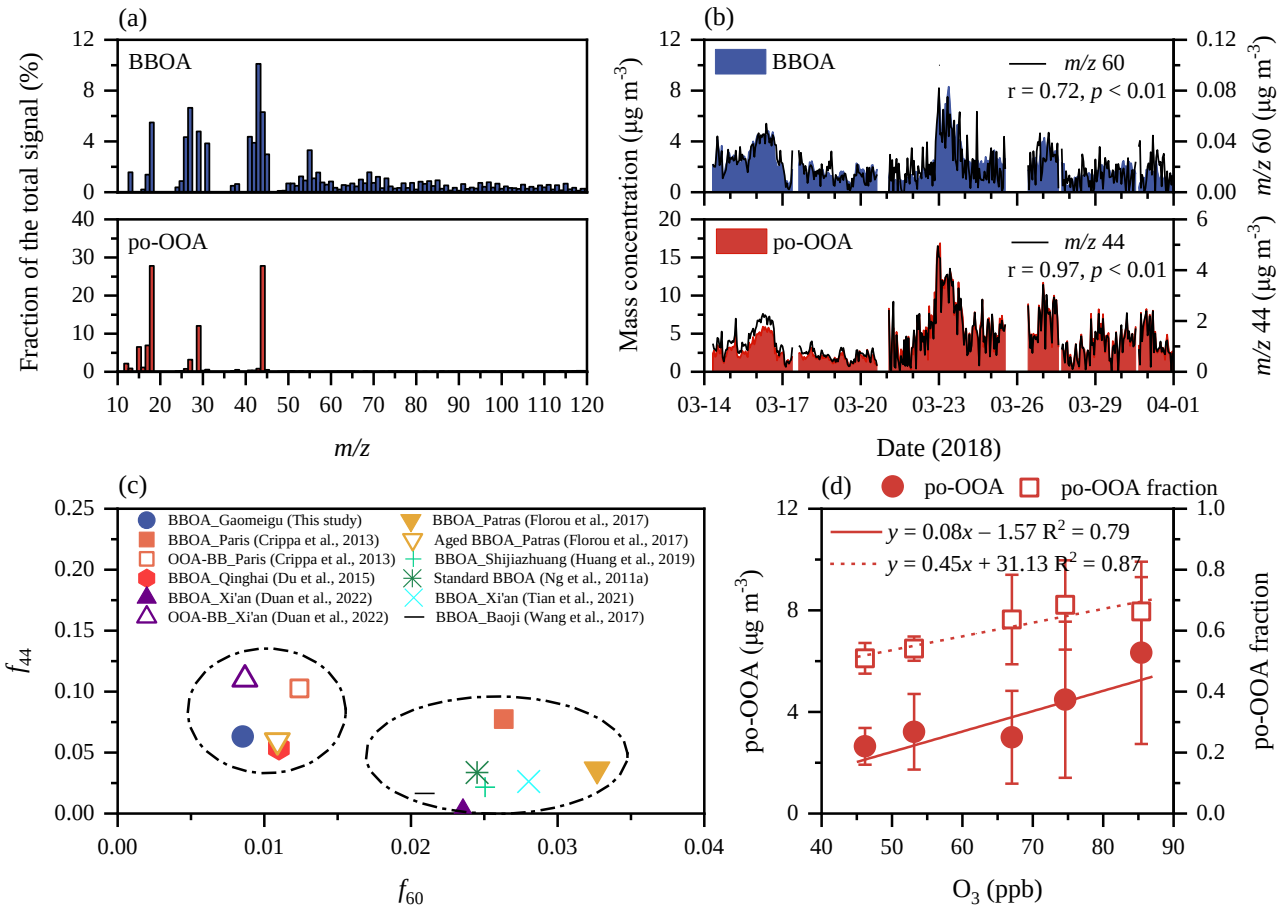

Figure 4. (a) Mass spectra of BBOA and po-OOA. (b) Pearson correlations between mass concentrations of OA components and the tracer molecular fragments. (c) Scatterplots of f_{44} vs. f_{60} for BBOA resolved in this study and reported by previous literatures. (d) Variations of po-OOA mass concentration and its fraction in OA as a function of O_3. The data are grouped in O_3 bins (10 ppb increment).

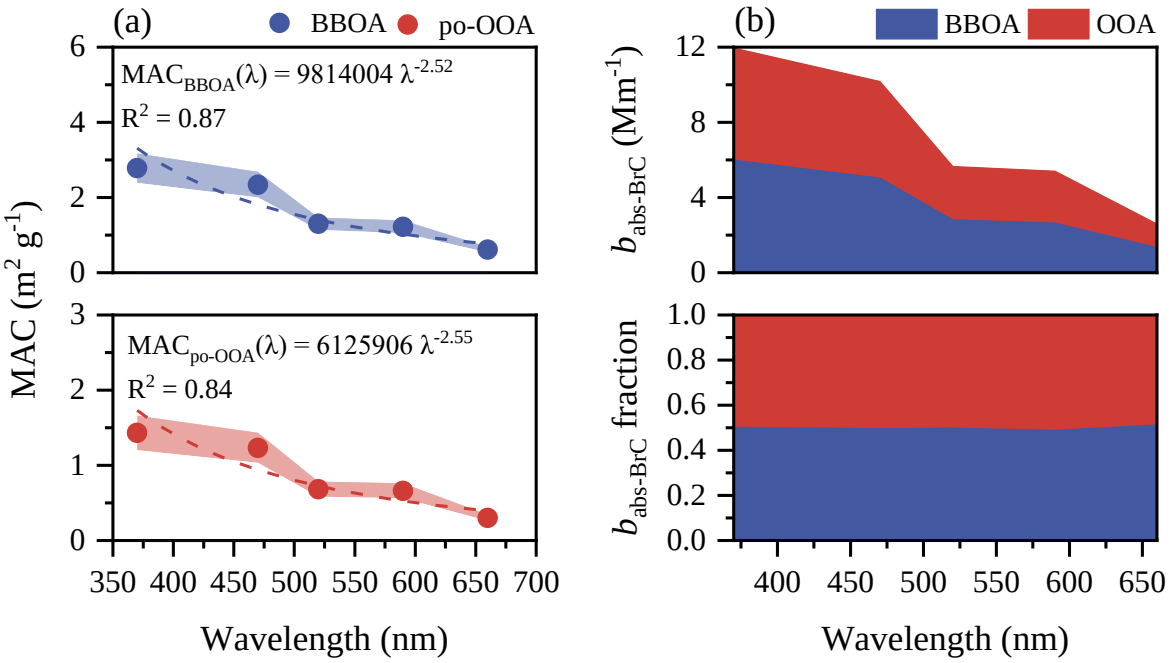

670

Figure 5. (a) The mass absorption cross section of BBOA and po-OOA (MAC_{BBOA} and $MAC_{po\text{-}OOA}$, respectively) at five wavelengths (λ = 370, 470, 520, 590, and 660 nm). The circle and shaded area represent the mean MAC values and the standard deviations, respectively. The dashed line is power-law fit. (b) Light absorption coefficient of BrC ($b_{abs\text{-}BrC}$) from BBOA and po-OOA and its fraction in the total reconstructed BrC absorption at different wavelengths.

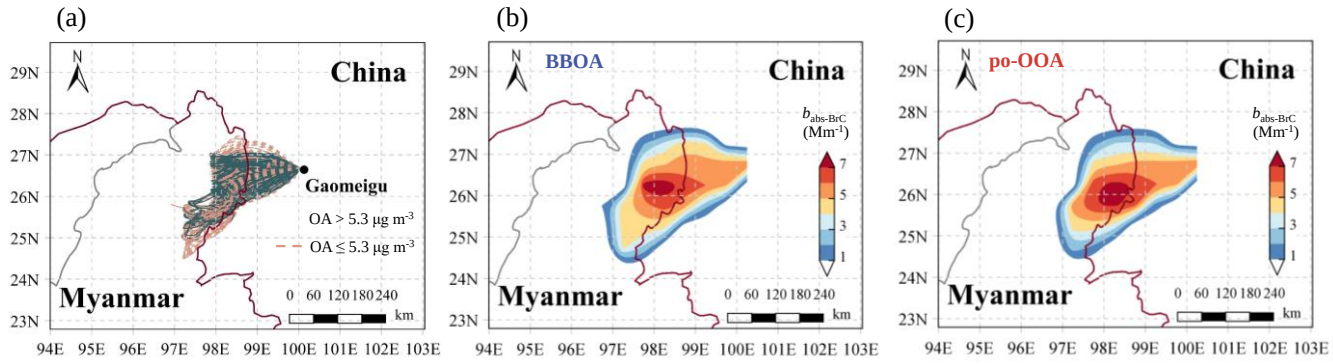

Figure 6. (a) 72-h backward trajectories of Gaomeigu from 8:00 on 14 to 23:00 on 31 March, 2018. (b) and (c) Concentration weighted trajectory (CWT) maps of $b_{abs\text{-}BrC}$ at 370 nm (Mm^{-1}) from BBOA and po-OOA, respectively.

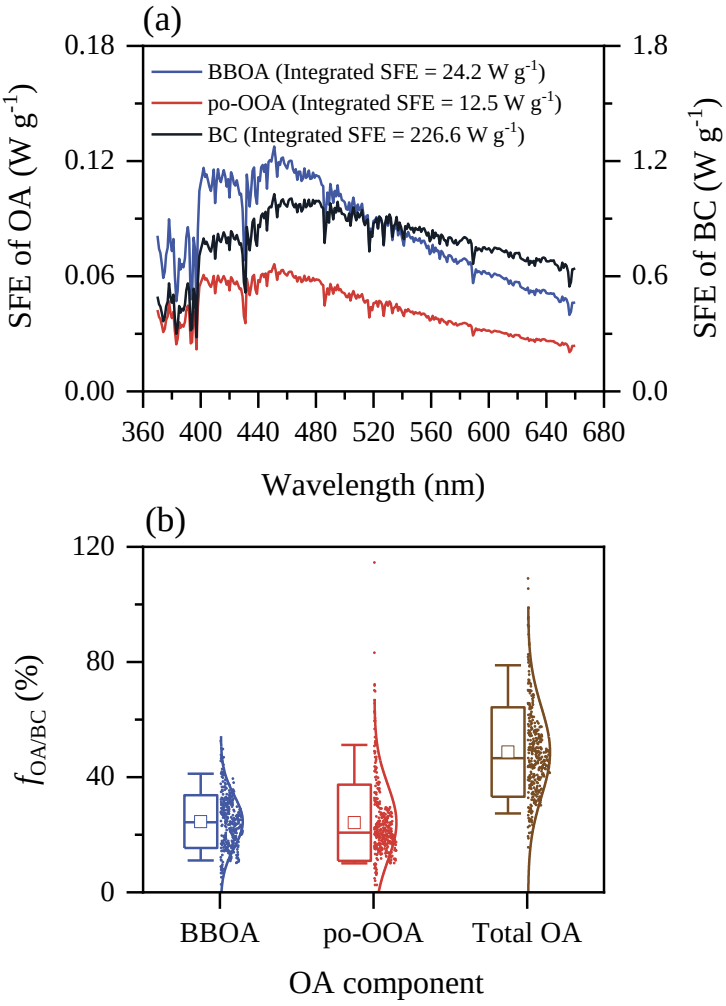

Figure 7. (a) Simple forcing efficiency (SFE) of light-absorbing particles from 370 to 660 nm and the integrated SFE over the entire solar spectra (370−660 nm). (b) The fraction of solar radiation absorbed by OA components relative to BC. In each panel, the short line and square inside the boxes indicate the median and mean values, respectively. The lower and upper edges of the boxes denote the standard deviation. The vertical bars ("whiskers") show the 5th and 95th percentiles. Scattered data points and normal distribution curve are also shown.